A Novel Achromatopsia Mouse Model Resulting From a Naturally Occurring Missense Change in Cngb3

Mark M. Hassall,[1,2] Alun R. Barnard,[1,2] Harry O. Orlans,[1,2] Michelle E. McClements,[1] Peter Charbel Issa,[1,2] Sher A. Aslam,[1,2] and Robert E. MacLaren[1,2]

[1]Nuffield Laboratory of Ophthalmology, Department of Clinical Neurosciences, University of Oxford, Oxford, United Kingdom
[2]Oxford Eye Hospital, Oxford University Hospitals NHS Foundation Trust, Oxford, United Kingdom

Correspondence: Mark M. Hassall, Nuffield Laboratory of Ophthalmology, Level 6, West Wing, John Radcliffe Hospital, Oxford OX3 9DU, UK;
m.hassall@gmail.com.
Alun R. Barnard, Nuffield Laboratory of Ophthalmology, Level 6, West Wing, John Radcliffe Hospital, Oxford OX3 9DU, UK;
alun.barnard@eye.ox.ac.uk.

Submitted: July 10, 2018
Accepted: November 21, 2018

Citation: Hassall MM, Barnard AR, Orlans HO, et al. A novel achromatopsia mouse model resulting from a naturally occurring missense change in Cngb3. *Invest Ophthalmol Vis Sci*. 2018;59:6102–6110. https://doi.org/10.1167/iovs.18-24328

Purpose. A local colony of inbred mice (129S6/SvEvTac origin), in isolation for over a decade, were found to have absent light-adapted electroretinogram (ERG) responses. We investigated the inheritance and genetic basis of this phenotype of cone photoreceptor function loss.

Methods. An affected 129S6/SvEvTac colony animal was outcrossed to a C57BL/6J mouse and intercrossed to investigate inheritance in the F2 generation. We performed ERG testing and targeted resequencing on genes of interest (*Gnat2*, *Cnga3*, *Cngb3*, *Pde6c*, *Hcn1*, *Syne2*). The eyes of a subset of animals underwent histologic immunostaining.

Results. All 129S6/SvEvTac colony animals tested lacked cone pathway function by ERG testing ($n = 12$), although rod pathway–based ERG responses remained unaffected. Outcross-intercross breeding showed a recessive inheritance pattern. A novel missense mutation was identified in the *Cngb3* gene, which causes an amino acid substitution at a conserved residue (NM_013927)c.692G>A; p.(R231H). The recessive phenotype only affected homozygotes ($\chi^2 = 39$, $P = 3.2e^{-10}$). Cones had normal morphology at postnatal day (PND) 70, but cone cell counts declined from PND 30 to PND 335 ($P = 0.038$), indicating progressive cone photoreceptor death.

Conclusions. We identified the spontaneous occurrence of a 10th model of cone photoreceptor function loss (*cpfl10*) in an isolated line of inbred mice. Our results indicate that this is caused by a novel missense mutation in the *Cngb3* gene, with a fully recessive inheritance pattern. This mouse may provide a more appropriate background against which to assess *CNGB3* achromatopsia gene therapy for missense mutations.

Keywords: retina, achromatopsia, Cngb3, cones

We noticed that a particular colony of inbred mice (of 129S6/SvEvTac origin) had poor light-adapted visual responses and hypothesized that a novel genetic mutation affecting cone photoreceptors might be responsible. Cone photoreceptors facilitate daytime vision, color perception, and central visual acuity.[1,2] The cone phototransduction cascade and homeostatic functioning of cones has multiple linked steps and a single cone gene mutation can cause loss of cone function.[3]

Mice are valuable for the identification and investigation of genes and mutations that may affect normal cone photoreceptor function, particularly in achromatopsia. There have been nine mouse models of cone photoreceptor function loss (*cpfl*) reported since *cpfl1* was first described (Chang B, et al. *IOVS* 2001;42:ARVO Abstract 527). The *cpfl* retinal phenotype varies across the models and the genetic basis is different for each. Yet, all nine models display the common trait of partial or complete loss of cone function from birth, sometimes with progressive cone cell loss (Chang B, et al. *IOVS* 2001;42:ARVO Abstract 527) (Hawes NL, et al. *IOVS* 2003;44:ARVO E-Abstract 4531) (Chang B, et al. *IOVS* 2006;47:ARVO E-Abstract 2294) (Hawes NL, et al. *IOVS* 2004;45:ARVO E-Abstract 3590) (Hawes NL, et al. *IOVS* 2006;47:ARVO E-Abstract 4579) (Hawes NL, et al. *IOVS* 2007;47:ARVO E-Abstract 1350) (Chang B, et al. *IOVS* 2015;ARVO E-Abstract B0250).[4,5] Mouse models also facilitate the development of retinal gene and molecular therapies; two *cpfl* models have been central in developing adeno-associated virus (AAV) gene therapies before trials in humans.[6,7] The *cpfl* phenotypes model human achromatopsia, a rare (1 in 30,000–80,000), congenital visual condition characterized by diminished or absent cone photoreceptor function.[8] Patients have severely reduced visual acuity (~20/200), nystagmus, and photophobia.[9] Causative autosomal recessive mutations largely affect genes of the cone phototransduction cascade and are summarized elsewhere.[10]

CNGB3 forms a heterotetramer cyclic nucleotide–gated (CNG) transmembrane channel with CNGA3 and is the most commonly affected gene in human achromatopsia.[11] CNGB3 is the minor component in direct channel conductance and plays a modulatory role.[12] In murine retinal sections, CNGB3 and CNGA3 colocalize and are expressed exclusively in cone photoreceptors.[13] CNGB1 and CNGA1 form an analogous CNG channel specific to rod photoreceptors.[14]

Here we described the *cpfl10* mouse phenotype in detail and identified the causative missense mutation in exon 6 of *Cngb3*, producing a substitution of histidine for arginine. We identified a slow degeneration of cones in this model and demonstrate that heterozygotes do not suffer any intermediate phenotype.

Copyright 2018 The Authors

This work is licensed under a Creative Commons Attribution-NonCommercial-NoDerivatives 4.0 International License.

Downloaded From: https://iovs.arvojournals.org/pdfaccess.ashx?url=/data/journals/iovs/937686/ on 01/07/2019

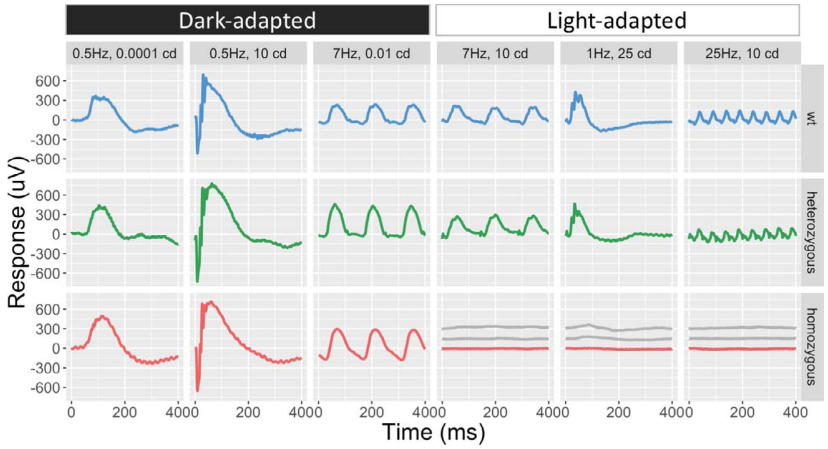

Figure 1. ERG results for individual mice genotyped as homozygous (*red*), heterozygous (*green*), or wild type (*blue*) for the (NM_013927)c.692G>A; p.(R231H) mutation. A range of scotopic rod-isolating, photopic cone-isolating, or mixed rod-cone test conditions are displayed. The additional *gray traces* in the final panels show the small residual cone response sometimes present in less than a quarter of *cpfl10* mice and F2 progeny.

Methods

Mice and Breeding

All animals used in this study were treated humanely in accordance with the UK Home Office Regulations and the ARVO Statement for the Use of Animals in Ophthalmic and Vision Research. Animals were housed in a 12:12 hour light-dark cycle. An affected 129S6/SvEvTac colony animal was outcrossed to a wild-type C57BL/6J mouse to produce first filial generation hybrid offspring (129SB6F1). The 129SB6F1 animals were intercrossed to investigate inheritance in the F2 generation. A further intercross of affected homozygous F2 offspring was performed to produce an F3 generation to confirm penetrance. Complementation breeding of an 129S6/SvEvTac mouse with a *Cnga3*$^{-/-}$ colony produced offspring to exclude *Cnga3* as a possible affected gene. In confocal scanning laser ophthalmoscopy (cSLO), optical coherence tomography (OCT), and qPCR experiments, mice from a commercially obtained 129S2/SvHsd colony (Envigo, Cambridgeshire, UK) were used as approximate strain-matched controls.

Electroretinography

Before the ERG procedure, mice were dark adapted (>1 hour) and the procedure was performed under dim red illumination. The mouse was anaesthetized with a single intraperitoneal injection (80 mg/kg ketamine and 10 mg/kg xylazine) and the pupils were dilated with tropicamide 1% and phenylephrine 2.5% eye drops. The mouse was positioned on a heated mat in front of the testing console (Colordome Electroretinography machine; Diagnosys LLC, Vision Park, Cambridge, UK), which also generated and controlled the light stimulus. Corneal electrodes (Diagnosys LLC) coupled with custom lenses produced from achromatic Aclar embedding (Honeywell International, Morris Plains, NJ, USA) were positioned on the cornea by using micromanipulators and viscous coupling media (Hypromellose 1%; Alcon, Fort Worth, TX, USA). Subcutaneous ground and reference electrodes (platinum needles) were placed in the flank and scalp.

The test protocol consisted of three dark-adapted and seven light-adapted steps. Dark-adapted recordings commenced with a dim single flash −4 log cd.s/m^2 stimuli, with an interstimulus interval (ISI) of 5 seconds, and averaged over 9 trials. A brighter single flash of 1 log cd.s/m^2 stimuli was also used, with an ISI of 30 seconds, and averaged over 4 trials. Continuous stimuli of 7 Hz were delivered at −2 log cd.s/m^2 and averaged over 30 responses. After dark-adapted recordings were completed, animals were exposed to a full-field 30 cd/m^2 white background for 10 minutes; subsequent steps were delivered on top of this continuous background. Single-flash stimuli after light adaptation consisted of −0.5, 0, 0.5, 1, and 1.5 log cd.s/m^2; 20 responses were averaged, with an ISI of 1 second. Continuous stimuli of 7 Hz and 20 Hz were delivered at 1 log cd.s/m^2 and averaged over 30 responses.

ERG a-wave and b-wave amplitudes were measured (Espion v6; Diagnosys LLC) by using manual and automated methods. Technically inadequate replicates of traces were excluded. A-wave and b-wave cursors were placed manually. Full b-wave amplitudes in rod-isolating test steps were measured from the trough of the a-wave to the peak of the b-wave. B-wave amplitudes in light-adapted test steps were measured from the amplitude at onset of stimulus to the peak of the b-wave. If the a-wave was undetectable then b-wave amplitude was measured from the baseline at stimulus onset.

cSLO and OCT

The retinal phenotype was assessed in vivo by using a combined confocal scanning laser ophthalmoscope and spectral-domain optical coherence tomograph (Spectralis HRA; Heidelberg Engineering, Heidelberg, Germany). Fundus autofluorescence imaging was performed by following a previously described protocol using 488- and 790-nm excitation light, and near-infrared reflectance imaging using a 820-nm laser.[15]

OCT captures cross-sectional images of the retina by using low-coherence interferometry of infrared light. The section density, orientation, and technical replicates of scan patterns were customized to include a high-definition linear scan and a radial scan. Total and outer retinal thickness measurements were made manually by using calipers on Heidelberg software.

Downloaded From: https://iovs.arvojournals.org/pdfaccess.ashx?url=/data/journals/iovs/937686/ on 01/07/2019

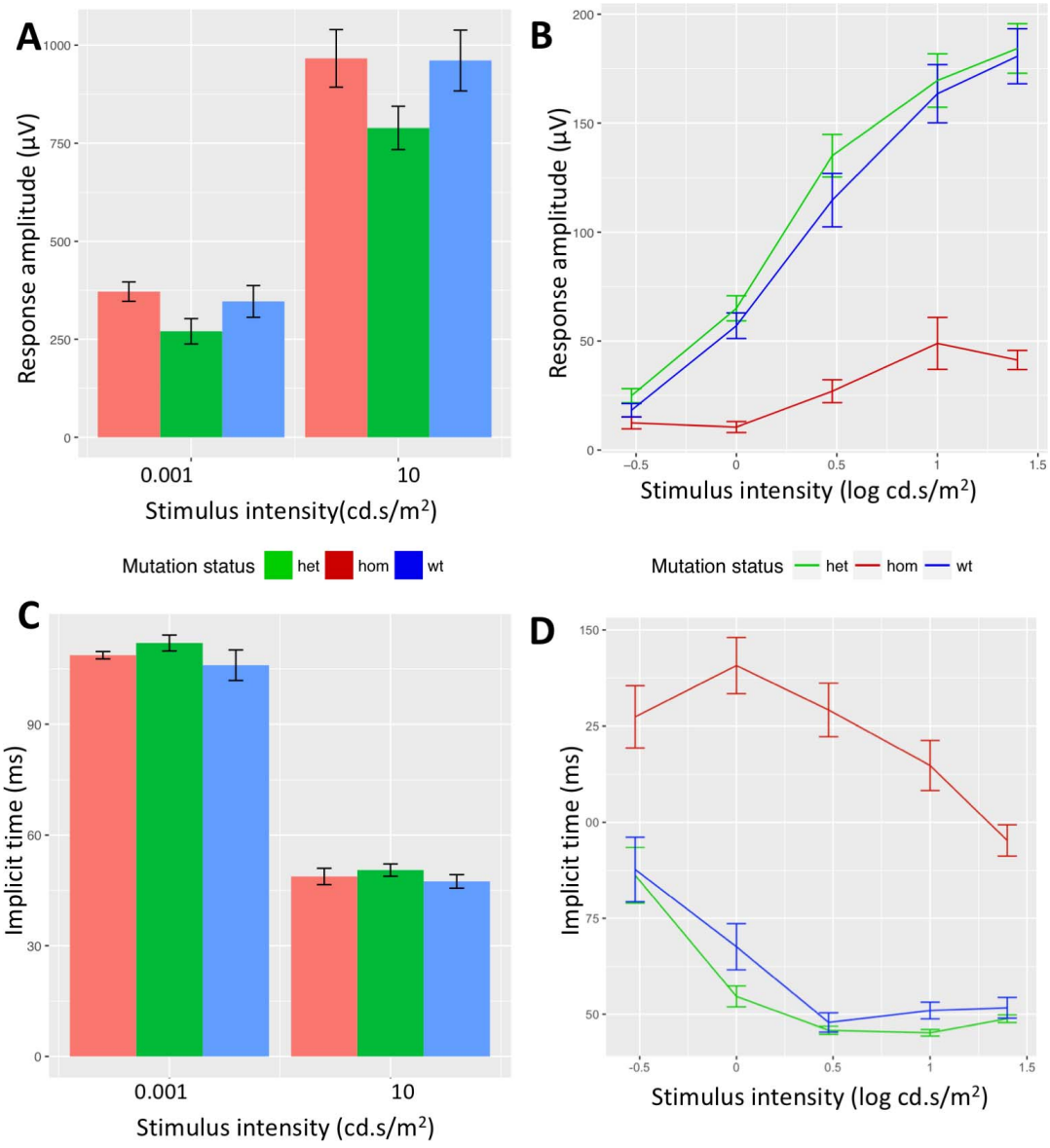

Figure 2. (**A**) B-wave amplitude for dark-adapted rod-isolating test steps in homozygous (hom, *red*), heterozygous (het, *green*), or wild-type (wt, *blue*) mice ($n = 65$). (**B**) The irradiance response curve (IRC) for B-wave amplitude in light-adapted cone-isolating ERG test steps ($n = 65$ mice consisting of 18 hom, 26 het, 21 wt) shows that heterozygous mice have normal cone function, yet homozygous mice have severely diminished cone response. (**C**) Rod b-wave implicit time does not vary. (**D**) Cone b-wave implicit time for the same mice shows no significant difference between heterozygous and wild-type. All values are mean of the group (μV or ms) ± SEM.

Targeted Resequencing, Genotyping, and Restriction Fragment Length Polymorphism (RFLP)

Tail tissue was collected and genomic DNA (gDNA) was extracted with a commercial DNA mini kit (QIAGEN, Manchester, UK). Custom primer pairs were designed to the reference coding sequence for *Gnat2*, *Cngb3*, and *Pde6c*. Initially, gDNA from six pilot mice was amplified with PCR and the target amplicon confirmed with agarose gel electrophoresis. The PCR product was extracted with a commercial kit according to the manufacturer's instructions. Samples underwent commercial fluorescent dideoxynucleic acid sequencing and the results were analyzed with Geneious v8.0 software (Biomatter, Auckland, New Zealand). Single nucleotide polymorphisms (SNPs) were compared to the National Center for Biotechnology Information (NCBI) dbSNP database; established SNPs were assessed as nonpathologic and not investigated further. The *Cngb3* base pair variation not documented on NCBI dbSNP was sequenced further in the full 77 mouse cohort of *cpfl10* ($n = 12$), F2 intercross ($n = 59$), and F3 intercross mice ($n = 6$) to confirm cosegregation with phenotype.

Sanger sequencing results were validated by a custom RFLP assay. Genomic DNA was amplified by using custom primers targeting *Cngb3* exon 6 (FW-5′-TTCTCTCCACACCAGTGCAC-3′ and RC-5′-ACACTGACAATGTTCTATCCACAGA-3′) and amplicons underwent restriction digest with *Apa*LI enzyme (NEB, Ipswich, MA, USA). On an agarose gel, wild-type mice showed bands at 454 bp and 15 bp, whereas homozygous mutants lacked the larger band and showed 267-bp, 187-bp, and 15-bp

Investigative Ophthalmology & Visual Science

Downloaded From: https://iovs.arvojournals.org/pdfaccess.ashx?url=/data/journals/iovs/937686/ on 01/07/2019

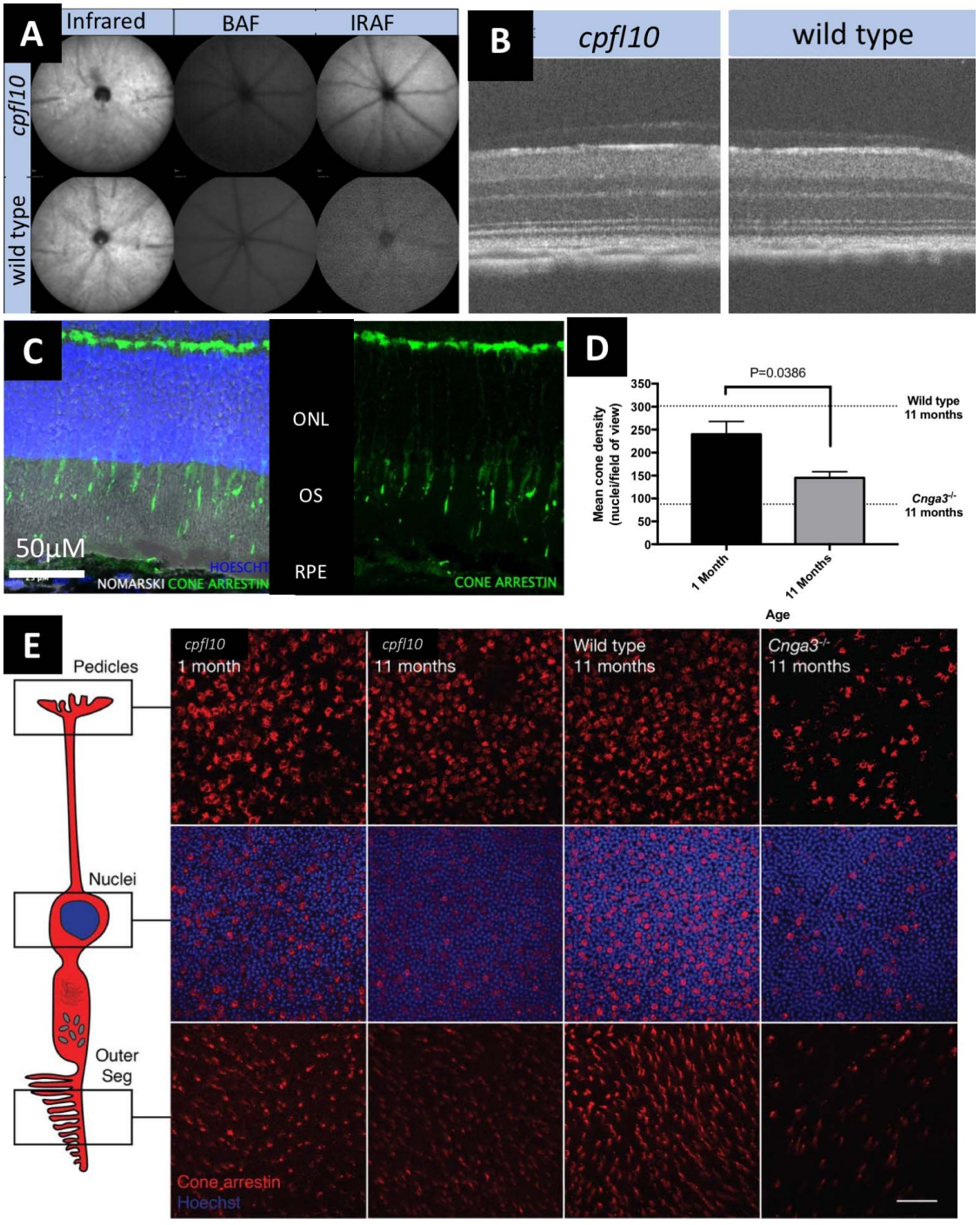

Figure 3. (**A**) Representative en face confocal scanning laser ophthalmoscopy images show no retinal changes indicating degeneration across all imaging modalities (PND 56). (**B**) Representative optical coherence tomography cross-sections show equal retinal thickness (PND 56) that is consistent across all mice measured ($n = 5$ *cpfl10* and $n = 5$ 126S/SvEvTac wild types). (**C**) Immunohistochemical staining for Arr3 in the *cpfl10* retina shows grossly normal cone morphology at PND 70 ($n = 4$ *cpfl10* eyes compared to $n = 2$ wild-type eyes). *Scale bar*: 50 µM. (**D**) The mean retinal cone count in *cpfl10* mice declines significantly from PND 30 to PND 335. (**E**) Representative retinal flat mounts with Arr3 staining showing the difference in cone number and morphology between *cpfl10* and controls. *Scale bar*: 10 µm.

Investigative Ophthalmology & Visual Science

Downloaded From: https://iovs.arvojournals.org/pdfaccess.ashx?url=/data/journals/iovs/937686/ on 01/07/2019

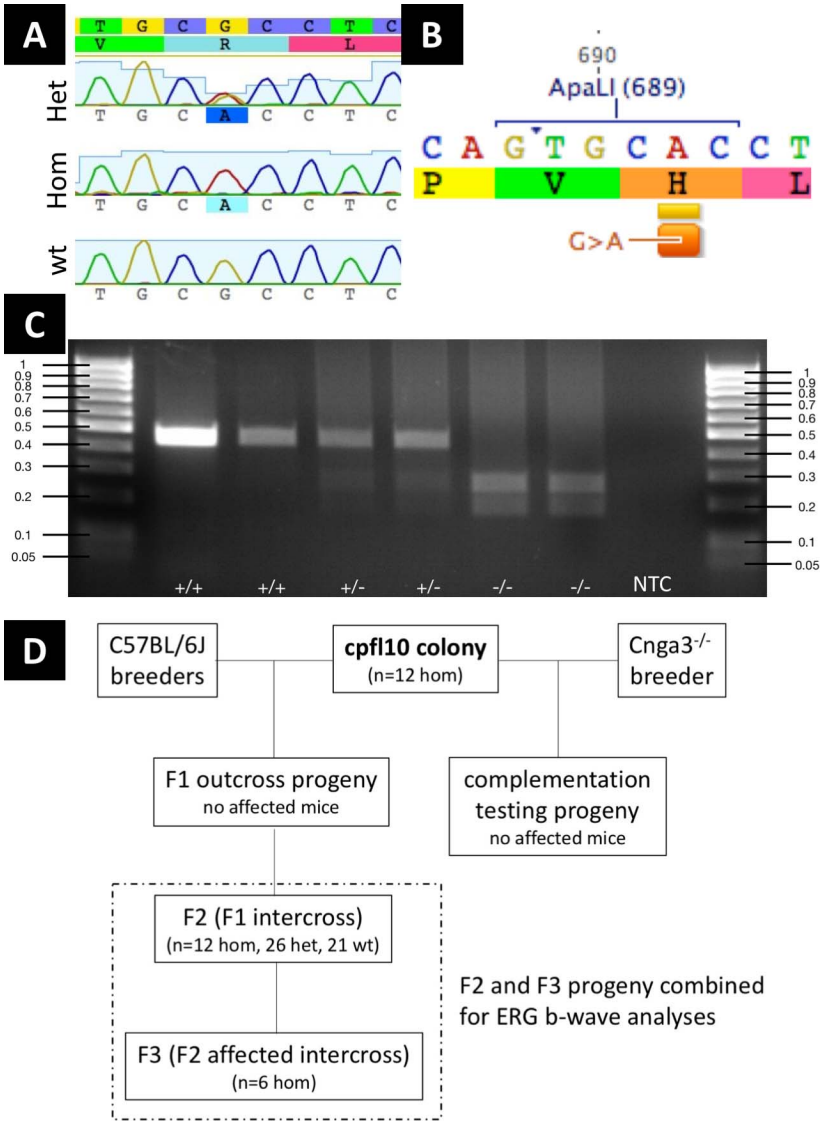

Figure 4. **(A)** The chromatogram for the c.692G>A mutation is shown for heterozygotes (*top*), homozygotes (*middle*), and wild-type littermates (*bottom*). **(B)** The c.692G>A mutation introduces a novel *Apa*LI restriction site in the *Cngb3* gene sequence. **(C)** An RFLP assay can thus identify homozygous, heterozygous, or wild-type mice; wt band = 469 bp, mutant band = 250 bp + 190 bp + 15 bp fragments. Sanger sequencing results for wt (+) or mutant (–) displayed below each lane show 100% concordance across all samples tested with RFLP ($n = 43$ animals assayed). NTC is negative template control, DNA ladder in kilobases. **(D)** A representation of the complementation and outcross breeding undertaken to identify the inheritance pattern of the *cpfl10* phenotype. The panel also lists the numbers of mice genotyped as heterozygous (het), homozygous (hom), or wild type for the c.692G>A missense mutation.

fragments—the G>A missense mutation introduced a new *Apa*LI cut site in the middle of the exon 6 amplicon (see Figs. 4B, 4C).

mRNA Extraction and qPCR

Retinal tissue was homogenized in a lysis solution of B-mercaptoethanol and chaotropic buffer. Passing the solution 10 times each through a 25-gauge and 30-gauge needle optimized homogenization. The solution was then bound to a silica-gel-membrane spin column by centrifugation. DNase was added to degrade contaminant DNA, before further wash steps with buffer. The RNA was eluted in water.

Eluted retinal RNA was reverse transcribed to cDNA by using the Superscript III synthesis system (Life Technologies, Paisley, UK) as per the manufacturer's instructions. cDNA was purified for PCR by using the QIAquick PCR purification kit (QIAGEN, Manchester, UK). Standard curve analysis was performed to ensure efficiencies were close to 100% and the optimal primer pairs for each gene were used (Table).

All qPCR reactions used a commercial kit (SYBR Green PCR Master Mix; Applied Biosystems, Foster City, CA, USA) and 2 μM final concentration of each forward and reverse primer. All qPCR experiments were performed in triplicate with a commercial real-time PCR machine (CFX Connect Optics Module; BioRad, Hercules, CA, USA). Reactions were performed with the following settings: an initial denaturation step of 95°C for 10 minutes, followed by 40 cycles of 95°C for 30 seconds, an annealing temperature of 55°C, and extension at 72°C for 30 seconds.

Investigative Ophthalmology & Visual Science

Downloaded From: https://iovs.arvojournals.org/pdfaccess.ashx?url=/data/journals/iovs/937686/ on 01/07/2019

Table. List of Primers Used in the Transcriptome Analysis

Gene	Direction	Nucleotide Sequence (5′–3′)
ActB	Forward	AGCCATGTACGTAGCCA
	Reverse	GAAGCTGTAGCCACGCT
Cnga3	Forward	TAGACATGCTGGTTCGAGC
	Reverse	GTTGGTCCTTGTCTCTGTG
Cngb3	Forward	AGCCAGCTCTCAGACTGCA
	Reverse	ACAGTTCCAGTTATACGCA
Rho	Forward	TGCTCAACTTGGCCGT
	Reverse	GCGGAAGTTGCTCATCG

Immunohistochemistry and Flat Mounts

Following euthanasia and enucleation, the cornea was excised at the limbus. The zonules were blunt dissected with Vannas scissors and the lens extruded whilst avoiding retinal traction. For cryosections, eyecups were transferred to 4% (wt/vol) PFA (Thermo Fisher Scientific, Waltham, MA, USA) for 30 minutes initial fixation and then sequentially transferred to 10%, 20%, and 30% sucrose. They were then embedded in OCT compound (VWR, Radnor, PA, USA) and stored at –80°C until sectioning. Sample blocks were sectioned in 20-µM slices at –22°C (Cryotome LSE; Thermo Fisher Scientific). For flat mounts, the neural retina was dissected from the eyecup and fixed in 4% PFA for 30 minutes. Both retinal sections and whole retinal cups were permeabilized with dilute Triton X-100, blocked with donkey serum, and incubated with primary anti-cone arrestin primary antibody (AB15282; Millipore, Burlington, MA, USA). Secondary staining was performed with Alexa-Fluor 568 donkey anti-rabbit (A10042; Thermo Fisher Scientific) and nuclei were stained with Hoechst 33342 (Thermo Fisher Scientific). Following staining, retinal cups were dissected into petaloid quarters until the tissue flattened uniformly. Both cryosection and flat mount slides were mounted in Prolong Diamond Antifade media (Thermo Fisher Scientific). All slides were then imaged on a confocal microscope (Leica Microsystems GmbH, Wetzlar, Germany). Cone counts were performed manually from confocal retinal flat mount fluorescence micrographs taken by using the ×40 objective in the nuclear plane. For each retina the mean number of nuclei per field of view was calculated from images centered within each of the four leaves of the mount.

Statistical Analysis

Statistical analysis was performed with R software (v3.4.1).[16] Inheritance pattern was analyzed by using Pearson's χ^2 test with Yates continuity correction. The difference between mean ERG b-wave amplitudes was analyzed by using mixed effects linear regression. qPCR data were analyzed by using the ΔΔCt method.[17] Nonlinear modelling of the sigmoidal ERG irradiance response curve and calculation of the mean asymptote were performed by using the nlme package in R.[18]

In silico analysis and modelling of (NM_013927)c.692G>A; p.(R231H) mutation was performed. The Visual Molecular Dynamics (VMD) freeware[19] was used in silico to assemble and analyze previously published models of mouse Cngb3 (UniProt: Q9JJZ9) and Human CNGB3 (UniProt: Q9NQW8). Cngb3 was also examined in context by using the Cngb3/a3 heterotetramer model (Swiss model ID: 5h3o.1) built from 3.5-Å-resolution single-particle electron cryomicroscopy structure of a cyclic nucleotide–gated channel from *Caenorhabditis elegans*.[20] Predictive scores for the deleterious effect of the arginine to histidine substitution were calculated by using the Poly-Phen II[21] and Protein Variation Effect Analyzer (PROVEAN)[22] web-based services.

Results

Functional and Structural Retinal Phenotype of the Mouse *cpfl10* Mutant

The *cpfl10* phenotype can be easily identified by ERG. For all mice tested in the original colony ($n = 12$), dark-adapted rod responses were equivalent to C57BL/6J wild-types (linear regression, $P = 0.4$), and light-adapted cone responses were completely absent or substantially reduced to 15% to 20% of littermate b-waves ($n = 12$ mice; Fig. 1). A further 114 mice derived from outcrosses and intercrosses of *cpfl10* were phenotyped. All of the original *cpfl10* mice ($n = 12$), the entire F2 cohort ($n = 59$), and the F3 intercross cohort ($n = 6$) were genotyped. Figure 2 gives detailed analysis of the F2 and F3 cohort ERG phenotype and the relationship to genotype.

The *cpfl10* retinal fundus appeared normal on all applied cSLO imaging modalities when compared with a commercially obtained 129S2/SvHsd colony (Envigo) wild type (Fig. 3A, investigated up to postnatal day [PND] 60). OCT assessment of the retinal layers showed normal architecture and thickness measurements that were not different when compared to wild type (194 ± 0.03 µM, 193 ± 0.09 µM; $P = 0.43$; Fig. 3B). Immunohistochemistry (IHC) staining for cone arrestin at PND 70 showed normal retinal appearance and cone morphology (Fig. 3C). However, retinal flat mounts stained for cone arrestin (Figs. 3D, 3E) in *cpfl10* mice at PND 30 ($n = 3$) and PND 335 ($n = 3$) showed a significant reduction in retinal cone counts over time ($P = 0.039$; *t*-test). The cone loss observed in *cpfl10* mice at PND 335 was far more severe than what might be expected for normal aging (145 ± 13 nuclei/field of view for *cpfl10* versus 302 ± 17.8 nuclei/field for approximately age and strain-matched controls). Yet, surviving cones in *cpfl10* mice were slightly more numerous than in age-matched mice from the *Cnga3*$^{-/-}$ line (87 ± 3 cone nuclei/field of view at PND 335), which is known to experience progressive cone photoreceptor loss.

Inheritance Pattern

Figure 4D shows that complementation breeding of the *cpfl10* mice with a *Cnga3*$^{-/-}$ colony produced offspring ($n = 21$) all with normal cone function on light-adapted ERG testing. The lack of complementation showed the *cpfl10* mutation is not allelic to *Cnga3* ($\chi^2 = 38.7$, $df = 1$, $P < 0.001$).

In outcrosses with C57BL/6J mice, the *cpfl10* phenotype occurred in an autosomal recessive pattern. None of the C57BL/6J outcross F1 progeny (129SB6F1) displayed a deficit in cone ERG function ($n = 28$), excluding a dominant inheritance pattern ($\chi^2 = 57$, $P < 0.001$). The F1 progeny were then intercrossed to each other to produce an F2 generation to further explore inheritance. Approximately one quarter in the F2 generation ($n = 15/59$) showed the original *cpfl10* phenotype, indicating an autosomal recessive inheritance pattern ($\chi^2 = 13$, $P < 0.001$). Intercross of two affected F2 mice showed full penetrance of the phenotype in the subsequent F3 generation ($n = 6$). The *cpfl10* ERG phenotype cosegregated with the c.692G>A mutation in 100% of mice sequenced ($\chi^2 = 39$, $P = 3.2e^{-10}$).

Mutation Analysis

Targeted resequencing revealed that affected mice did not carry any of the spontaneous *cpfl* mutations previously described. No mutations were detected in affected mice during sequencing of the entire coding sequence of *Gnat2*—the known *Gnat2*^{cpfl3} exon 6 mutation was excluded (Chang B, et al. *IOVS* 2001;42:ARVO Abstract 527). No mutations were

Investigative Ophthalmology & Visual Science

Downloaded From: https://iovs.arvojournals.org/pdfaccess.ashx?url=/data/journals/iovs/937686/ on 01/07/2019

found in those exons of *Hcn1* gDNA that were sequenced (approximately 70% of exons), which had been previously linked to achromatopsia (Chang B, et al. *IOVS* 2006;47:ARVO E-Abstract 2294). Further sequencing of the remaining *Hcn1* exonic gDNA was stopped once the causative mutation was found in the *Cngb3* gene. The *Syne2* mutation (c.13978C>T; p.Q4660*) was excluded.[5] *Cnga3* was not sequenced, as it was excluded earlier by complementation testing.

A novel missense mutation, c.692G>A; (p.Arg231His), was identified in exon 6 of the *Cngb3* gene. The mutation introduces a unique *Apa*LI restriction site that can be exploited in a genotyping RFLP assay to confirm the Sanger sequencing results (Fig. 4). There are no other known *cpfl* genes located on chromosome 4 along with *Cngb3* that could cosegregate.

The arginine at position 231 is the first extracellular amino acid immediately adjacent to the first transmembrane domain of the CNGB3 protein and is highly conserved across species (Fig. 5A). The arginine residue in the same location in CNGA3 is also conserved across species (Fig. 5B). Fewer than 25% of residues are conserved between both CNGA3 and CNGB3 across multiple species. The CNG channels are heterotetramers and thus important residues and protein domains share similarities between both component proteins. The location of the affected residue within the larger structure of CNGB3 and the heterotetramer is displayed in Figures 5C and 5D.

In silico analysis of the mouse mutation predicted a "deleterious" effect, with a PROVEAN score of −4.985, well beyond the cutoff of −2.5. Based on cross-species conservation, the predicted human mutation (NM_019098)c.764G>A; p.(R239H) was explored by using peer-reviewed Poly-Phen II in silico tools and a score of 1.000 predicted this equivalent mutation to be "probably damaging" in humans.

Effect of *cpfl10* Mutation on mRNA and Protein Expression

Regarding mRNA, retinal samples from *cpfl10* mice ($n = 5$ *cpfl10* mice; PND 84) and controls ($n = 3$ 129S2/SvHsd mice [Envigo]; PND 80) expressed both *Cngb3* and *Cnga3* transcripts on qPCR. After normalization to the *ActB* reference gene, *Cngb3* expression levels in *cpfl10* mice were similar to controls ($\Delta\Delta$Ct = 0.83 ± 0.85; $P = 0.262$). Expressed as a ratio, *Cngb3* expression in control mice was 1.7 ± 0.95 times greater than *Cnga3* ($P = 0.003$, Fig. 5E). In *cpfl10* mice, the *Cngb3* transcript expression levels were 3.3 ± 0.94 times higher than *Cnga3* levels ($P < 0.001$), a ratio that was significantly higher than controls ($P = 0.037$). However, the *Rho* levels of *cpfl10* mice were significantly lower than controls ($\Delta\Delta$Ct = 0.56 ± 0.85, $P = 0.011$), which suggests more extensive strain-related differences in the retinal transcriptome beyond the effects of the *cpfl10* mutation.

Regarding protein, the previously described *Cngb3* knockout mouse does not produce CNGB3 protein.[12] The CNGB3 IHC performed after successful AAV.*CNGB3* gene therapy rescue of this model was performed by using a custom-generated antibody that is not commercially available. All three commercially available antibodies to human CNGB3 (ABIN571515, Antibodies Online, Atlanta, GA, USA; CPBT 31596RH, Creative Diagnostics, Shirley, NY, USA; Orb156415, Biorbyt, Cambridge, UK) were tested on wild-type murine retinal sections at a range of concentrations. A nonspecific binding pattern was observed that could not be improved with optimization steps. Therefore, the protein expression of Cngb3 in the *cpfl10* mouse is currently unknown.

Discussion

This is the first naturally occurring mouse model of achromatopsia resulting from a mutation in *Cngb3*. A spontaneously occurring G>A nucleotide substitution in exon 6 of *Cngb3* mutates a conserved arginine residue. The missense mutation is located at the beginning of the first extracellular loop of the B-subunit of the cone-specific cyclic nucleotide–gated ion channel. In silico analysis on multiple platforms confirms a deleterious effect across species for mutations at this residue.

Normal cone function is lost in *Cngb3*$^{cpfl10/cpfl10}$ mice. The extent of cone function loss is potentially more severe than the incomplete achromatopsia observed in the previously published *Cngb3*$^{-/-}$ (Cngb3^{tm1Dgen}) mouse. This model contains a targeted deletion in exon 6, resulting in a premature stop codon c.733_749del; (p.A247*), and yet still reliably retains 20% to 30% of wild-type ERG function.[23] This may arise because the CNGA3 subunits form a channel on their own. It is also possible that truncated CNGB3 is still translated and contributing to function—the authors have used a far C-terminal antibody that would be unable to detect truncated products.[23] Notably, the *cpfl10* model involves a slow progressive cone degeneration over the first year, which has been observed in other models of achromatopsia such as the *cpfl5* mouse.[24] Adaptive optic retinal imaging in human *CNGB3* and *CNGA3* achromatopsia cases has shown a slow decline in foveal cone density and changes in cone reflectivity throughout life.[25] In both the *cpfl10* mouse and human cases, cones survive long enough to provide a therapeutic window for treatment.

CNGB3 forms a heterotetramer cyclic nucleotide–gated transmembrane channel with CNGA3.[13] The subunit configuration of cone CNG channels is thought to be either 3A:1B or an equal 2A:2A configuration, although homomeric 4A channels can form in vitro.[26,27] A mutant CNGB3 could therefore impair function by altering normal subunit ratios, interfering with subunit assembly, preventing heterotetramer insertion in the cell membrane, or affecting heterotetramer functioning after assembly. The transcriptome results showing increased *Cngb3* expression in the *cpfl10* mouse could be consistent with increased promoter induction in response to reduced CNGB3 protein.

Theoretically, a diminished ability of the mutant membrane channel to fully open or fully close could therefore impair hyperpolarization in the cone phototransduction cascade. The affected arginine residue is 1 of only 48 residues in human CNGB3 conserved across all vertebrates. Missense mutations account for 4% of all human *CNGB3* achromatopsia mutations, but there are currently no reported human cases of mutation at this residue.[11] The incidence of achromatopsia in the Pinegelap islander population is approximately 10% due to a CNGB3 missense mutation at a highly conserved residue: c.1304C>T; (p.S433F). The *Cngb3*^{cpfl10} mouse model may provide a more appropriate preclinical model for developing genetic treatments for missense mutations in humans than the existing *Cngb3*$^{-/-}$ (Cngb3^{tm1Dgen}) mouse model.

Furthermore, this model may be beneficial in further exploring and understanding any differences in treatment effect observed in subgroups of patients (missense versus truncation mutations) in the current *CNGB3* phase I clinical trials in humans (NCT03001310 and NCT02599922). For example, *CNGB3* gene therapy vectors might be more effective in cases of premature stop codons rather than missense mutations. Such a difference could be explored through a direct comparison of AAV in the different missense (*cpfl10*) and truncation mouse models of *Cngb3* achromatopsia.

Investigative Ophthalmology & Visual Science

Downloaded From: https://iovs.arvojournals.org/pdfaccess.ashx?url=/data/journals/iovs/937686/ on 01/07/2019

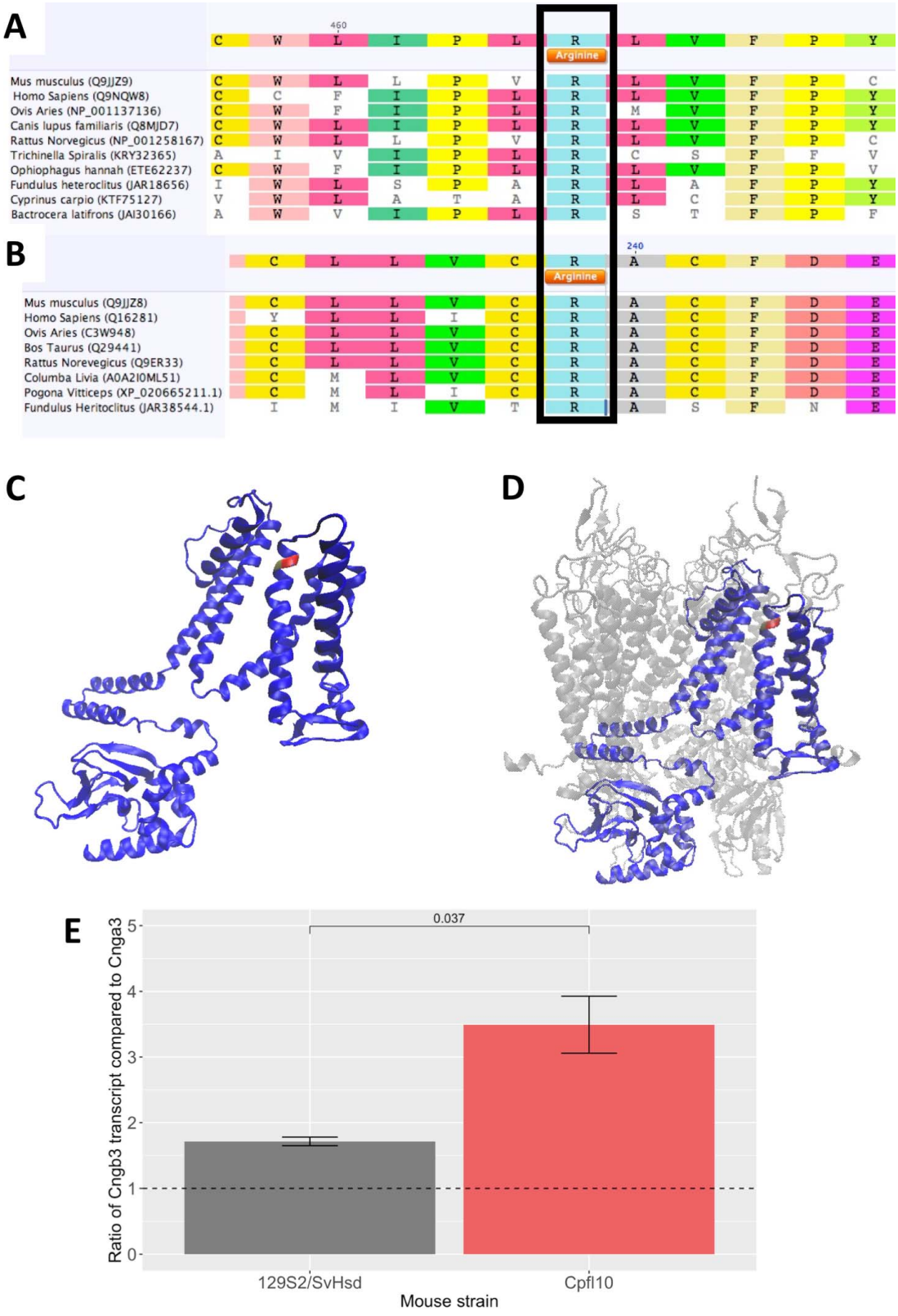

Figure 5. (**A**) The p.(R231H) missense mutation occurs at an arginine residue conserved across all vertebrates (within *black box*). (**B**) The equivalent arginine residue in Cnga3 is also highly conserved across vertebrates and other more distant species. (**C**) Structural modelling of Cngb3 shows the affected first residue of the first extracellular loop (red residue) and (**D**) in the context of the CNG heterotetramer. (**E**) The ratio of *Cngb3* transcript expression normalized to *Cnga3* transcript expression (*dotted line*) in *cpfl10* ($n = 5$; PND 84) and 129S2/SvHsd control mice ($n = 3$; PND 80) as measured with qPCR. Values are mean ± SEM.

Investigative Ophthalmology & Visual Science

Downloaded From: https://iovs.arvojournals.org/pdfaccess.ashx?url=/data/journals/iovs/937686/ on 01/07/2019

Acknowledgments

Supported by the Amar-Frances and Foster-Jenkins trust.

Disclosure: **M.M. Hassall**, None; **A.R. Barnard**, None; **H.O. Orlans**, None; **M.E. McClements**, None; **P. Charbel Issa**, None; **S.A. Aslam**, None; **R.E. MacLaren**, None

References

1. Schnapf JL, Kraft TW, Baylor DA. Spectral sensitivity of human cone photoreceptors. *Nature*. 1987;325:439–441.
2. Mustafi D, Engel AH, Palczewski K. Structure of cone photoreceptors. *Prog Retin Eye Res*. 2009;28:289–302.
3. Larhammar D, Nordström K, Larsson TA. Evolution of vertebrate rod and cone phototransduction genes. *Philos Trans R Soc Lond B Biol Sci*. 2009;364:2867–2880.
4. Chang B, Dacey MS, Hawes NL, et al. Cone photoreceptor function loss-3, a novel mouse model of achromatopsia due to a mutation in Gnat2. *Invest Ophthalmol Vis Sci*. 2006;47:5017–5021.
5. Maddox DM, Collin GB, Ikeda A, et al. A mutation in Syne2 causes early retinal defects in photoreceptors, secondary neurons, and Müller glia. *Invest Ophthalmol Vis Sci*. 2015;56:3776–3787.
6. Carvalho LS, Xu J, Pearson RA, et al. Long-term and age-dependent restoration of visual function in a mouse model of CNGB3-associated achromatopsia following gene therapy. *Hum Mol Genet*. 2011;20:3161–3175.
7. Alexander JJ, Umino Y, Everhart D, et al. Restoration of cone vision in a mouse model of achromatopsia. *Nat Med*. 2007;13:685–687.
8. Michaelides M, Hunt DM, Moore AT. The cone dysfunction syndromes. *Br J Ophthalmol*. 2004;88:291–297.
9. Simunovic MP, Moore AT. The cone dystrophies. *Eye*. 1998;12:553–565.
10. Hassall MM, Barnard AR, MacLaren RE. Gene therapy for color blindness. *Yale J Biol Med*. 2017;90:543–551.
11. Mayer AK, Van Cauwenbergh C, Rother C, et al. CNGB3 mutation spectrum including copy number variations in 485 achromatopsia patients. *Hum Mutat*. 2017;38:1579–1591.
12. Kaupp UB, Seifert R. Cyclic nucleotide-gated ion channels. *Physiol Rev*. 2002;82:769–824.
13. Matveev AV, Quiambao AB, Browning Fitzgerald J, Ding X-Q. Native cone photoreceptor cyclic nucleotide-gated channel is a heterotetrameric complex comprising both CNGA3 and CNGB3: a study using the cone-dominant retina of Nrl–/– mice. *J Neurochem*. 2008;106:2042–2055.
14. Weitz D, Ficek N, Kremmer E, Bauer PJ, Kaupp UB. Subunit stoichiometry of the CNG channel of rod photoreceptors. *Neuron*. 2002;36:881–889.
15. Charbel Issa P, Singh MS, Lipinski DM, et al. Optimization of in vivo confocal autofluorescence imaging of the ocular fundus in mice and its application to models of human retinal degeneration. *Invest Ophthalmol Vis Sci*. 2012;53:1066–1075.
16. R Core Team. R: A Language and Environment for Statistical Computing. 2017. https://www.R-project.org/. Accessed November 29, 2017.
17. Schmittgen TD, Livak KJ. Analyzing real-time PCR data by the comparative C(T) method. *Nat Protoc*. 2008;3:1101–1108.
18. Pinheiro JC, Bates DM. Linear mixed-effects models: basic concepts and examples. In: *Mixed-Effects Models in S and S-PLUS. Statistics and Computing*. Springer, New York, NY; 2000:3–56.
19. Humphrey W, Dalke A, Schulten K. VMD: visual molecular dynamics. *J Mol Graph*. 1996;14:33–38.
20. Li M, Zhou X, Wang S, et al. Structure of a eukaryotic cyclic-nucleotide-gated channel. *Nature*. 2017;542:60–65.
21. Adzhubei IA, Schmidt S, Peshkin L, et al. A method and server for predicting damaging missense mutations. *Nat Methods*. 2010;7:248–249.
22. Choi Y, Chan AP. PROVEAN web server: a tool to predict the functional effect of amino acid substitutions and indels. *Bioinformatics*. 2015;31:2745–2747.
23. Ding X-Q, Harry CS, Umino Y, Matveev AV, Fliesler SJ, Barlow RB. Impaired cone function and cone degeneration resulting from CNGB3 deficiency: down-regulation of CNGA3 biosynthesis as a potential mechanism. *Hum Mol Genet*. 2009;18:4770–4780.
24. Pang J-J, Deng W-T, Dai X, et al. AAV-mediated cone rescue in a naturally occurring mouse model of CNGA3-achromatopsia. *PLoS One*. 2012;7:e35250.
25. Georgiou M, Kalitzeos A, Patterson EJ, Dubra A, Carroll J, Michaelides M. Adaptive optics imaging of inherited retinal diseases. *Br J Ophthalmol*. 2018;102:1028–1035.
26. Zhong H, Molday LL, Molday RS, Yau K-W. The heteromeric cyclic nucleotide-gated channel adopts a 3A:1B stoichiometry. *Nature*. 2002;420:193–198.
27. Peng C, Rich ED, Varnum MD. Subunit configuration of heteromeric cone cyclic nucleotide-gated channels. *Neuron*. 2004;42:401–410.

Investigative Ophthalmology & Visual Science

Downloaded From: https://iovs.arvojournals.org/pdfaccess.ashx?url=/data/journals/iovs/937686/ on 01/07/2019